Electroluminescence Radiance Maps based on Multiple Exposure Images from InGaAs Cameras

Mantel, Claire; Spataru, Sergiu Viorel; Del Prado Santamaria, Rodrigo; Poulsen, Peter Behrensdorff; Benatto, Gisele Alves dos Reis; Forchhammer, Søren

Published in:
Proceedings of the 8th World Conference on Photovoltaic Energy Conversion

Link to article, DOI:
10.4229/WCPEC-82022-2BV.2.47

Publication date:
2022

Document Version
Peer reviewed version

ELECTROLUMINESCENCE RADIANCE MAPS BASED ON MULTIPLE EXPOSURE IMAGES FROM INGAAS CAMERAS

Claire Mantel[1], Sergiu V. Spataru*[2], Rodrigo Del Prado Santamaría[2], Peter Behrensdorff Poulsen[2], Gisele Alves dos Reis Benatto[2], Søren Forchhammer[1]
[1]DTU Fotonik, Kgs. Lyngby, Denmark, [2]DTU Fotonik, Roskilde, Denmark

ABSTRACT: This paper presents a method to increase the dynamic range of the EL signal for diagnostics of defective areas in PV modules. It applies a computational method for reconstructing a high dynamic range radiance map from a stack of standard dynamic range images at multiple exposure times designed by Debevec and Malik for visible light cameras (RGB). Increasing the precision of the EL signal has two interests: more quantitative information is then available for automatic analysis, and better visual quality is available for visual inspection in case of a small amplitude EL signal, such as acquired in an outdoor daylight setup using lock-in EL. Both are demonstrated via two experiments during which a PV module is electrically biased and imaged at 8 different exposure times with an InGaAs camera: one indoor and one outdoor in daylight. The exposure times are combined to reconstruct an EL image of higher precision. To measure the increased precision, the number of unique pixel values is used: it increases by a factor larger than 2.5 for the indoor case and a factor higher than 100 in the outdoor case. In the outdoor case the improvement towards visual inspection is also clearly apparent.

Keywords: Electroluminescence, Defects, Experimental methods, Evaluation, Reliability

1 INTRODUCTION

This paper focuses on the usage of electroluminescence (EL) images from InGaAs cameras for diagnostic of photovoltaic (PV) cells in a PV module. Since the first presentation of EL imaging for inspection of PV modules [1], advancements have been made allowing its usage outdoor in daylight [2] or towards faster inspection using for example drones [3].

The purpose is here to achieve a better precision of the EL signal in terms of amplitude at each pixel. Achieving a finer granularity on the EL signal provides more information on the variation of the EL signal and is interesting in two regards: added information will help automatic analysis and diagnostic algorithms and, in the case of a low EL signal amplitude, increasing the signal granularity will also help for visual inspection by making more details visible. That second aspect is for example relevant for outdoor daylight EL-based inspection of solar installations [2], for example using drones to acquire images [3]. Indeed, in such cases, the range of the EL image obtained by computing the difference between electrically biased and background images can be rather small. For instance, it has been shown to be lower than 100 values for images taken outdoor under global horizontal irradiance (GHI) of approximately 670 W/m^2 [4].

As a finer granularity in a signal can be seen as a larger dynamic range, we use an approach designed for visible light cameras that aims at retrieving the high dynamic range radiance map of a scene from a stack of standard dynamic range images acquired at different exposure times [5]. That approach operates in two steps. First, the response function of the camera is determined, modeling the relation between the product of the radiant flux incident on the sensor and exposure time and the pixel value. In a second step, a high dynamic range image of the radiant flux at each pixel is reconstructed, up to a scaling factor. An advantage of using such data-based methods is to limit the a priori knowledge on the camera system and environment.

The article is organized in the following way: first the original method is presented in Sec. 2. It is then applied on datasets acquired during two experiments: one performed indoor (without noise due to sunlight) and one performed outdoor using electrical modulation and image processing to retrieve the EL signal [2]. The experiments are presented along with the obtained results in Sec. 3 for the indoor setup and Sec. 4 for the outdoor setup, respectively.

2 PREVIOUS WORK

One usage of EL images of PV modules is to estimate optoelectronic characteristics of the modules such as the diffusion length of minority carriers [1] or series resistance [6]. Some models exist describing the relationship between the characteristics of a solar cell and an EL image of it [6]. In [6], the authors include in their model the camera system using a priori knowledge such as the quantum efficiency or gain of the camera. The method presented here is another way to estimate the emitted flux incident on the sensor using several images with multiple exposure times but no other prior knowledge about the camera. The result achieved is determined up to a scaling factor and therefore needs a reference point for absolute calibration (e.g. a specific light source like in [7]). As the sensitivity of a camera depends on environmental factors such as its temperature, this data-based approach can adapt more easily to the current condition of the camera and is therefore quite flexible.

In practice, we have adapted image processing techniques that reconstruct a large dynamic range radiance map using multiple images taken with standard dynamic range at multiple exposure times. Those techniques were developed for visible light cameras (RGB), as opposed to InGaAs cameras in our case, and are assuming that the content of the scene imaged is static. The principle of this

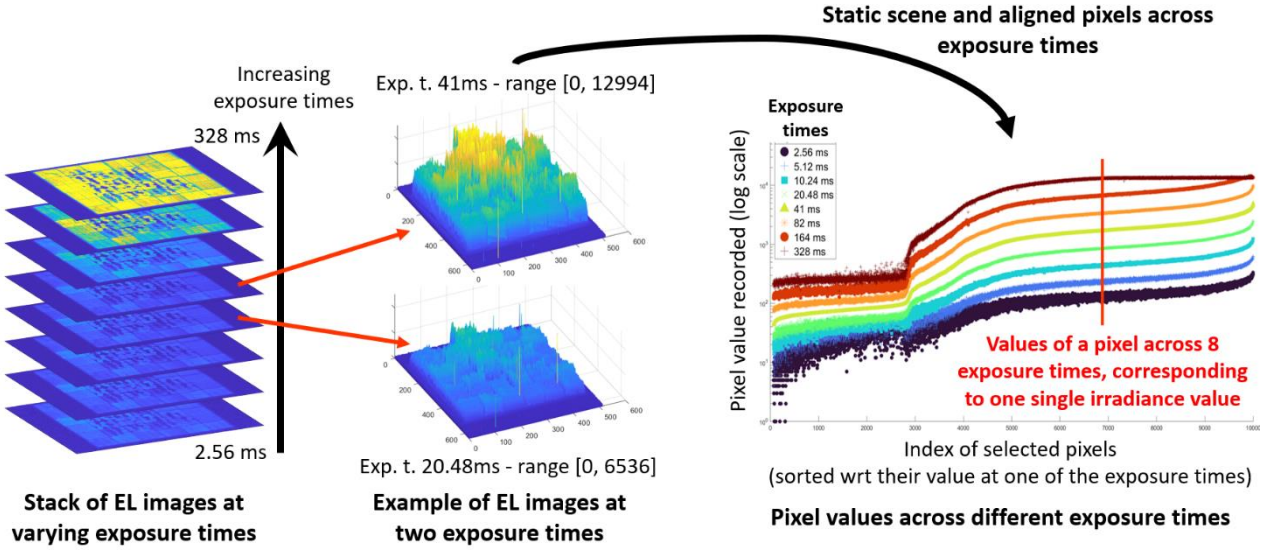

Figure 1 Data structure of multiple exposure time EL images and its utilisation in the reconstruction method from [5]

process was first presented by Debevec and Malik in [5]. The way the stack of images at multiple exposure times are used is illustrated in Figure 1.

The main idea is that for a specific pixel, the digital value issued by a camera depends on the camera response, the radiant flux received on the sensor and the exposure time of the sensor. Using the assumption that the radiant flux on each pixel is constant, it is possible to compute the response of a camera to the product of a specific radiant flux by the exposure time. Once this camera response function is computed, it is possible to retrieve, up to a scaling factor, the radiant flux incident on each pixel with a higher precision. To deduce fully the emitted flux, one also needs to account for other factors modifying the flux before it is incident on the sensor, such as vignetting of the lens of the camera or the transmittance of the atmosphere [6].

The modeling of the pixel response Z_{ij} in [5] is: $Z_{ij} = f(\varphi_i \times t_j)$ where f is a non linear function (the camera response), φ_i is the irradiance (radiant flux received by the sensor area) and t_j the exposure time.

By posing $g = ln(f^{-1})$, the problem can be reformulated as solving for g that minimizes the following cost, C:

$$C = \sum_{i=1}^{N}\sum_{j=1}^{P}\left[g(Z_{ij}) - \ln(\varphi_i) - \ln(\Delta t_j)\right]^2 + \lambda \sum_{z=Z_{min}+1}^{Z_{max}-1} g''(z)^2 \quad (1)$$

where N is the number of pixels, P the number of different exposure times and Z_{min} and Z_{max} the smallest and largest possible pixel values, respectively. The second term is added for regularization, with λ controlling the smoothness of the response. The logarithm of the inverse response function, g, needs to be resolved for the values between Z_{min} and Z_{max}.

The assumption that the radiant flux is constant on each pixel implies both that the scene is static across the acquisitions at all exposure times and that the pixels are registered across all exposure times.

3 INDOOR EXPERIMENT

3.1 Dataset

For the indoor experiment, a dataset of EL images at 16 exposure times was acquired. The module imaged is a 36 cells mechanically stressed multi-crystalline silicon module that was current biased at 100% I_{SC}. The InGaAs camera used for the experiment is a Raptor OWL 640 which has the following characteristics: resolution 640x512, spectral sensitivity 0.4µm to 1.7µm, pixel pitch 15mm x 15mm and readout noise (RMS) at low gain: <195 electrons. It uses active TEC cooling to keep the sensor at stabilized temperature. The lens mounted on it is a SWIRECON 25 mm SWIR lens.

The exposure time can be set to a minimum of 1 µs. To scan the whole dynamic range of the scene, 16 different exposure times were used for acquisition, with a x2 factor between each: [0.8, 0.16, 0.32, 0.64, 1.28, 2.56, 5.12, 10.24, 20.48, 41, 82, 164, 328, 656, 1312, 2624] ms. The acquisition was performed indoor without any daylight and 5 repeats of each exposure time were acquired. The lowest exposure times present a high amount of noise and the highest exposure times present saturated pixels. Only the 8 best exposure times 6 to 13 [2.56, 5.12, 10.24, 20.48, 41, 82, 164, 328] ms are included in the analysis below as their combination achieves the best result.

The input images were averaged over the 5 repetitions to remove part of the acquisition noise and then rounded to the nearest integer. The results are depicted in Figure 2. The images are scaled to the displayable range [0, 255] for better visualization whereas the actual range of values in each image is indicated above. It should be noted that there can be large differences between displayable and actual range of values.

3.2 Results

In practice, we solved Equation (1) for a subset of 10000 pixels randomly selected within the module and a smoothing parameter λ=3. The implementation was that available in [5], that is based on Singular Value Decomposition to solve the equation system, modified to handle input images with a bitdepth higher than 8 bits.

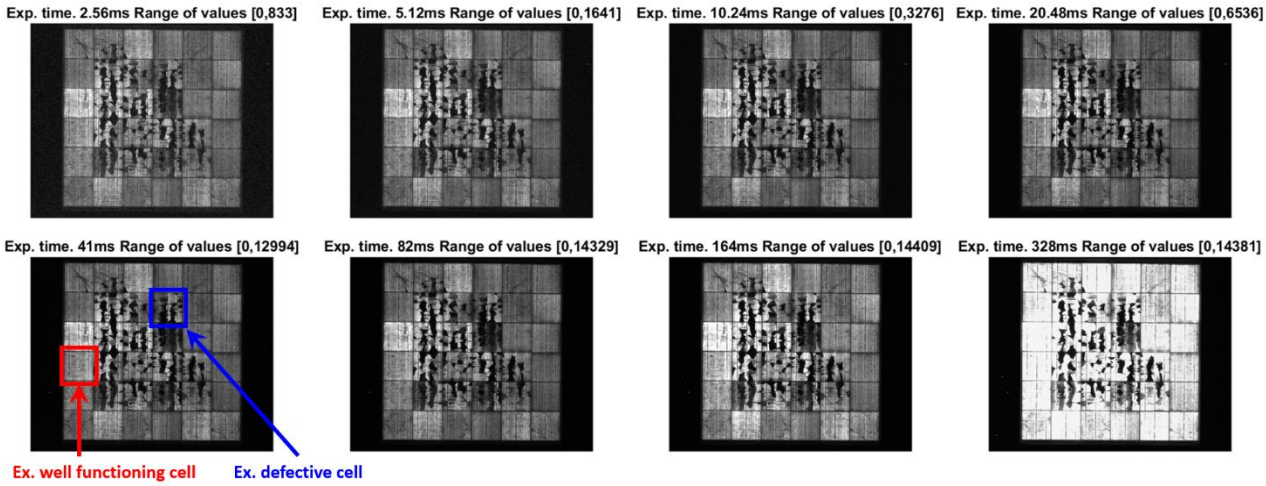

Figure 2: EL indoor images at the exposure times selected. The acquired images have been averaged over the 5 repeats and rounded. The range of values is indicated above each image and they are scaled between their 0.001 and 0.999 quantiles for visualization. The two cells selected for illustrating results are highlighted: in red for the well-functioning one and blue for the defective example.

Once the response function of our InGaAs camera is computed, the radiance map is reconstructed (using functions from [8] modified for higher bitdepth).

Results are shown in Figure 3 for a well-functioning cell, the one highlighted in red in Figure 2, and in Figure 4 for a cell presenting important defects, the one highlighted in blue in Figure 2 .

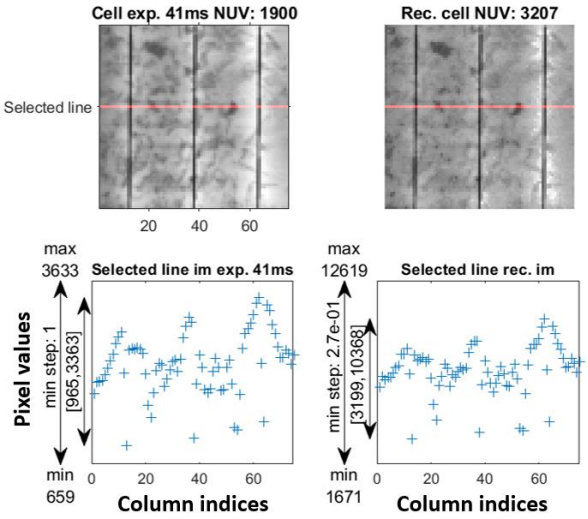

Figure 3: Example of best acquired (i.e. 41 ms exposure time, left) and reconstructed (right) images for a well-functioning cell (highlighted in red on Figure 1) with the corresponding number of unique value (NUV). In the second row, the profile of a selected line illustrates the interest of the method with regard to the minimum step size estimated and total cell variation.

In both cases, both a camera acquired image and the reconstruction are shown. The camera acquired image used here is the "best case scenario": i.e. the one with the highest possible exposure time that does not saturate (exposure time of 41 ms in our experiment which reaches a maximum value of 12994). It should be noted that the number of pixel values represented in Figure 3 and Figure 4 is limited to 256 (as [0, 255] is the standard range of displays), which is much lower than the real range of pixel values present in the images (up to 5500).

3.3 Analysis of results

The results are evaluated by comparing the EL image at 41 ms, i.e. the "best case" directly acquired EL, and the reconstructed EL image with a larger dynamic range. It is done both qualitatively through visual inspection of the EL images and quantitatively through the number of unique pixel values (NUV) and minimal step size present in the images.

As noted, the range of the figures presented here is much smaller than the full range of the images ([0, 255] as opposed to [0, >5000]). As it is also more than what the human eye is able to perceive without adaptation, the images at the top row of both Figure 3 and 4 appear similar. In this context of indoor imaging, when it is possible to acquire EL images with a large dynamic range, the method presented is not useful for visual inspection when looking at the whole cell. In case of zoom over a smaller portion of the image as done in the second row of Figure 4, the higher dynamic range can allow seeing ore details in both bright and dark areas. It here visible hereon the close up on a defective area (images 1 and 3 of the second row): the EL image at 41ms presents less details than the reconstructed EL (their dynamic range are [88, 211] and [114, 615], respectively).

It is however useful for automatic detection and analysis of defects. Indeed, the graphs on the bottom row of both Figures 3 and 4 show a higher number of NUV (increased by more than 2.5 times) and smaller step sizes obtained for the case of the reconstructed images (to the right). Automatic detection algorithms will leverage the finer step size to separate more accurately areas with optimal performance from those not functional in defective solar cells. In the middle row of Figure 4, an example of how automatic selection of inactive cell area based of EL signal could use the added information, both to identify defective areas and evaluate the level of defect within such a defective area.

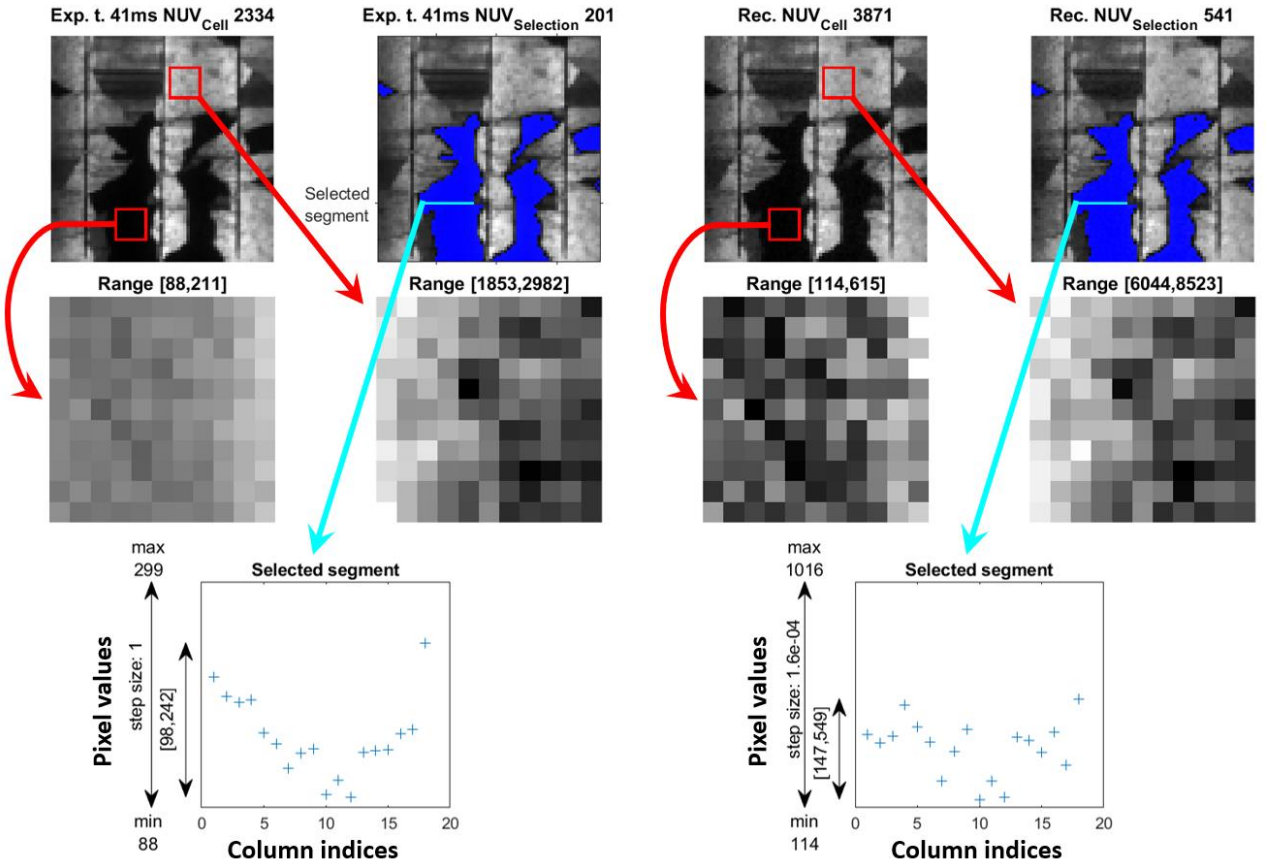

Figure 4: Example of best acquired (i.e. 41 ms exposure time, two leftmost columns) and reconstructed (two rightmost columns) images for a cell presenting significant defects (highlighted in blue on Figure 1). The first row depicts the images and a selected area representing the largest loss in terms of EL signal (highlighted in blue) and indicates their respective NUV. The second row focuses on zooms within the cell to illustrate the interest of higher dynamic range: finer granularity of values to make details visible in both dark and bright areas. The third row presents the profile of the selected segment to illustrate the interest of the method with regard to the minimum step size estimated and variation within the selected area.

4 OUTDOOR EXPERIMENT

4.1 Dataset

For the outdoor experiment, the same module as for the indoor experiment was imaged with the same InGaAs camera and lens. The camera was operating at 120Hz.

As the acquisition was performed in daylight (GHI was measured at 639 W/m^2 and the irradiance in the plane of array 71 W/m^2), the panel was electrically modulated for reconstruction [2] and a bandpass filter from Edmund Optics was used (25 nm band width, 1150 center wavelength, optical density 4). The module was biased at 100% I_{SC} with a square wave signal at 30Hz. The acquisition consisted in 2 electrically biased images followed by 2 unbiased images, also called background. 200 images were acquired at each exposure time, yielding 100 biased images and 100 background images.

Some processing was necessary to retrieve the electroluminescence signal. First, the corners of the module were detected, and the image cropped to the area of interest [9]. Then the images sequence was separated into biased and background images so the averaging over each category could be performed, before computing the difference [2].

Series of 200 images were acquired at the following 16 exposure time: [0.05, 0.08, 0.12, 0.18, 0.27, 0.398, 0.589, 0.87, 1.28, 1.9, 2.82, 4.17, 6.17, 9.13, 13.5, 20] ms. The exposure times were calculated as 14 points on a logarithmic scale between the lower bound representing a signal visible but noisy and the higher bound presenting saturation in the module area. An example of an image acquired and the retrieved EL image are depicted in Figure 5.

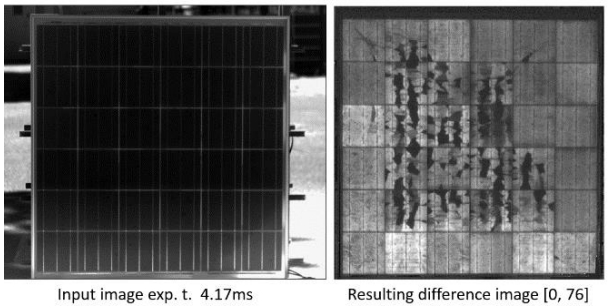

Figure 5: Example of outdoor SWIR image at exposure time 4.17 ms (left) and resulting EL image after module detection, BEL/BG identification, averaging and difference (right).

Due to the relative strength of the EL signal with regards to the noise and sun variation, a subset of 8 exposure times were selected to achieve the best results. Table I below presents the exposure times selected and the corresponding range of values present in the acquired SWIR image and the resulting EL images.

Table I: Selected exposure times and corresponding range of values in difference image for outdoor DS

Exp. Time (ms)	SWIR Image range	Difference image range
0.398	[396,4150]	[0, 20]
0.589	[546,6109]	[0, 21]
0.87	[791,9025]	[0, 29]
1.28	[1156,12970]	[0, 41]
1.9	[1587,14479]	[0, 53]
2.82	[1586,14479]	[0, 56]
4.17	[1634,14622]	[0, 76]
6.17	[1714,14655]	[0, 104]

4.2 Results

The same process was applied to reconstruct a larger dynamic range image for the 8 EL images at various exposure times: random selection of 10 000 pixels, solving of Equation (1) with smoothing parameter λ=3 using code adapted from [5] and reconstruction of EL image with adapted code from [8]. The obtained EL image is depicted in Figure 6.

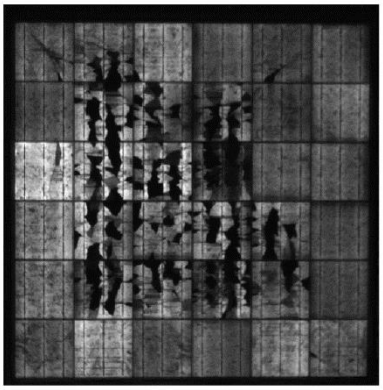

Figure 6: Larger dynamic range EL image obtained from 8 EL images at exposure times ranging from 0.398 ms to 6.17 ms.

Detailed results for the same cells as for the indoor experiment (Sec. 3) are presented hereafter: in Figure 7 for the well-functioning cell and in Figure 8 for the defective cell.

4.3 Analysis of results

The usefulness of the method is in that case evident both in terms of NUV but also visually. Indeed, the best achieved EL signal obtained through averaging and differencing (left column of Figure 7 and 8) presents clearly less information for visual inspection than the reconstructed larger dynamic range EL image using 8 exposure times (right column of Figure 7and 8). The second row of Figure 8 illustrates the interest of higher dynamic range for visual inspection when the input EL signal obtained by difference has a low amplitude by showing that more details are visible either in dark or bright areas.

When comparing with results from Sec. 3, it is apparent that the difference lies mainly in the quality of the EL images acquired outdoor. Indeed, the maximal amplitude of the EL image obtained through averaging and differencing between the electrically biased images and the background images is only around 100, as opposed to more than 14000 for the indoor experiment. The main reason for that limitation is that the amplitude of the EL signal in the SWIR images is low in comparison of the rest

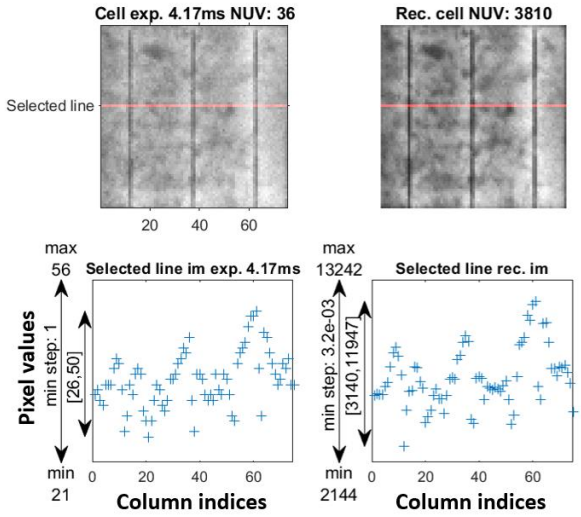

Figure 7: Example of best acquired (i.e. 4.17 ms exposure time, left) and reconstructed (right) images for a well-functioning cell (highlighted in red on Figure 1) with the corresponding NUV. In the second row, the profile of a selected line illustrates the interest of the method with regard to the minimum step size estimated and total cell variation.

of the image.

In the same way as shown for the indoor case, the increase in NUV and decrease in step size indicate that these results will allow more accurate automatic cell defect and fault detection in daylight EL images. In this case of low amplitude EL input signal, the NUV is increased by a factor higher than 100.

5 CONCLUSION AND FUTURE WORK

This paper applies a method designed for visible light cameras that combines images of a static scene acquired at different exposure times to retrieve an irradiance map of the scene with a larger dynamic range.

Reconstructing a larger dynamic range version of an EL image can be used to increase the available information for analysis and diagnostic of EL images of PV modules in the case of both automatic and visual inspections.

Both cases are illustrated through two experiments and evaluated through both the quantitative characteristics of the EL images and their visual aspect.

An indoor experiment using images acquired at 8 different exposure times is first presented. In that case the full range of the camera is used for the EL signal, which then presents a large range of values (more than 14000 in our case). The presented method is interesting for automatic inspection as the precision of the EL signal is increased, as measured by an increase factor of 2.5 to 5 in NUV and decrease 10^{-4} for the minimal variation present in the image.

An outdoor experiment allows illustrating the interests for both automatic and visual inspection. In this case the range of the camera is used for the complete SWIR image, i.e. both the EL signal and the unwanted noise due to the sunlight. Therefore, the EL signal obtained through averaging and differencing from EL lock-in input presents a rather small range of values (at most 104 for our experiment performed at 639 W/m^2 global irradiance and 71 W/m^2 POA). The image reconstructed using the presented method produces then a clear interest both for visual inspection and in terms of number of unique pixel

values (multiplied by more than 100 in that case).

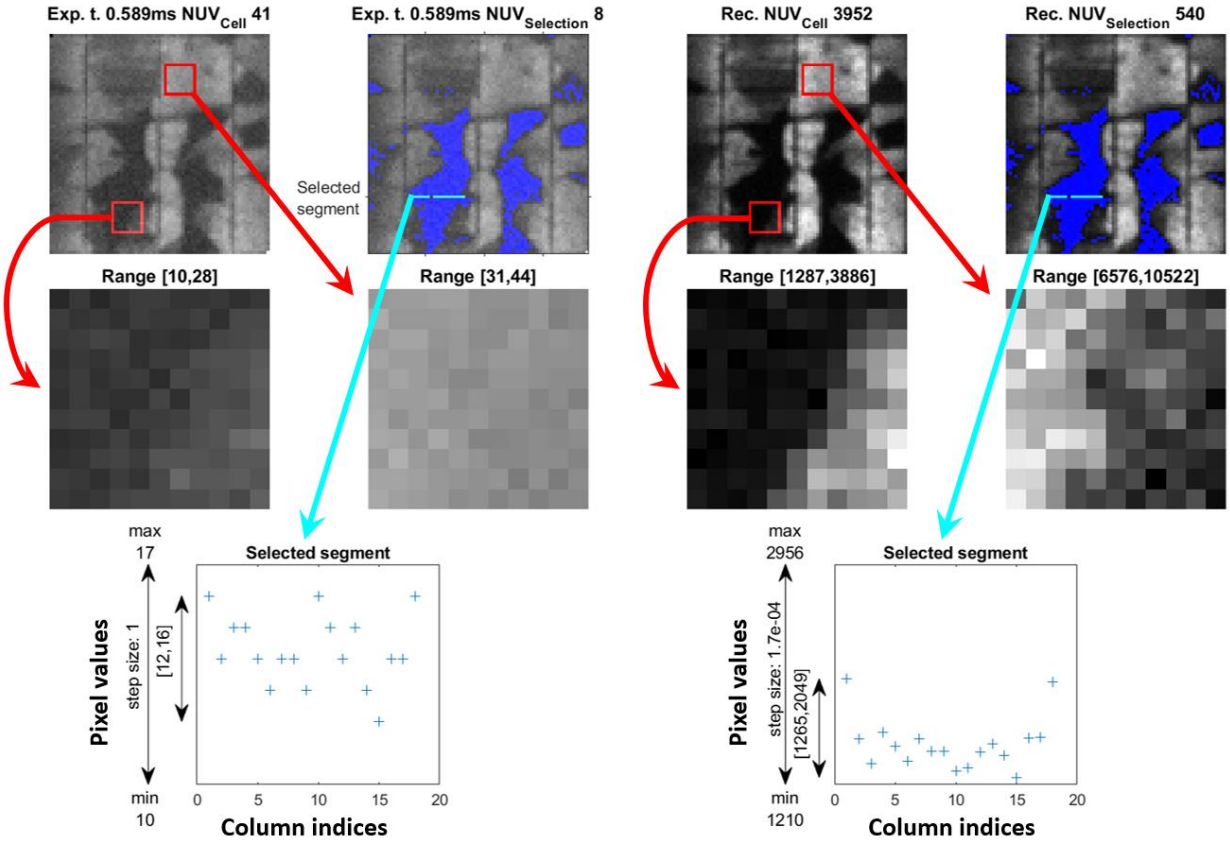

Figure 8: Example of best acquired (i.e. 4.17 ms exposure time, left) and reconstructed (right) images for a cell presenting significant defects (highlighted in blue on Figure 1). The first row depicts the images and a selected area representing the largest loss in terms of EL signal (highlighted in blue) and indicates their respective NUV. The second row focuses on zooms within the cell to illustrate the interest of higher dynamic range: finer granularity of values to make details visible in both dark and bright areas. The third row presents the profile of the selected segment to illustrate the interest of the method with regard to the minimum step size estimated and variation within the selected area.

6 ACKNOWLEDGMENTS

This research has been carried in the project DronEl2 project under the EUDP - Energy Technology Development and Demonstration Program with grant number 64019-0603.

7 REFERENCES

[1] T. Fuyuki et al., “Photographic surveying of minority carrier diffusion length in polycrystalline silicon solar cells by electroluminescence,” Applied Physics Letters, 2005

[2] L. Stoicescu, et al., “Daysy: luminescence imaging of pv modules in daylight,” in 29th European photovoltaic solar energy conference and exhibition proceedings (EU PVSEC), 2014

[3] G. Benatto et al., “Drone-Based Daylight Electroluminescence Imaging of PV Modules”. IEEE Journal of Photovoltaics, 2020

[4] Mantel, C et al., “SNR Study of Outdoor Electroluminescence Images under High Sun Irradiation”, In Proceedings of 7th World Conference on Photovoltaic Energy Conversion, 2018

[5] P. E. Debevec, J. Malik, “Recovering high dynamic range radiance maps from photographs”, in: Proceedings of ACM SIGGRAPH, 1997

[6] D. Ory et al., "Extended quantitative characterization of solar cell from calibrated voltage-dependent electroluminescence imaging", Journal of Applied Physics, 2021

[7] Mochizuki et al., "Solar-cell radiance standard for absolute electroluminescence measurements and open-circuit voltage mapping of silicon solar modules", Journal of Applied Physics, 2016

[8] Banterle, F. et al., “Advanced High Dynamic Range Imaging (2nd Edition)”, AK Peters (CRC Press), July 2017

[9] Mantel, C., et al., “Method for Estimation and Correction of Perspective Distortion of Electroluminescence Images of Photovoltaic Panels”, IEEE Journal of Photovoltaics, 2020